

RECEIVED: March 3, 2025 REVISED: April 17, 2025 ACCEPTED: May 5, 2025 PUBLISHED: June 18, 2025

Top-quark spin correlations as a tool to distinguish pseudoscalar $A \to ZH$ and scalar $H \to ZA$ signatures in $Zt\bar{t}$ final states at the LHC

Francisco Arco, a Thomas Biekötter, Panagiotis Stylianou, and Georg Weiglein, Panagiotis Stylianou,

Notkestr. 85, 22607 Hamburg, Germany

Calle Nicolás Cabrera 13-15, Cantoblanco, 28049, Madrid, Spain

Luruper Chaussee 149, 22761 Hamburg, Germany

E-mail: francisco.arco@desy.de, thomas.biekoetter@desy.de, panagiotis.stylianou@desy.de, georg.weiglein@desy.de

ABSTRACT: Both ATLAS and CMS have recently performed the first searches for a heavy new spin-0 resonance decaying into a lighter new spin-0 resonance and a Z boson, where the lighter spin-0 resonance subsequently decays into $t\bar{t}$ pairs. These searches are of particular interest to probe Two Higgs doublet model (2HDM) parameter space regions that predict a strong first-order electroweak phase transition. In the absence of CP violation, the investigated decay is possible if the lighter and the heavier spin-0 particles have opposite CP parities. The analysis techniques employed by ATLAS and CMS do not distinguish between the two possible signatures $A \to ZH$ and $H \to ZA$, where A and H denote CP-odd and CP-even Higgs bosons, respectively, if both signals are predicted to have the same total cross sections. We demonstrate the capability of angular variables that are sensitive to spin correlations of the top quarks to differentiate between $A \to ZH$ and $H \to ZA$ decays, even in scenarios where both signals possess identical total cross sections. Focusing on masses of 600 GeV and 800 GeV as a representative 2HDM benchmark, we find that a distinction between the two possible channels is possible with high significance with the anticipated data from the high-luminosity LHC, if the invariant mass distribution of the $t\bar{t}$ system is further binned in angular variables defined by the direction of flight of the leptons produced in the top-quark decays. Moreover, we find a moderate gain in experimental sensitivity due to the improved background rejection for both signals.

KEYWORDS: Multi-Higgs Models, Specific BSM Phenomenology

ARXIV EPRINT: 2502.03443

 $[^]a Deutsches\ Elektronen-Synchrotron\ DESY,$

^bInstituto de Física Teórica UAM/CSIC,

 $[^]c II.\ Institut\ f\"ur\ Theoretische\ Physik,\ Universit\"at\ Hamburg,$

18

18

1	Introduction	1
2	Theoretical framework and simulation	3
	2.1 The 2HDM	4
	2.2 Angular variables	6
	2.3 Monte Carlo simulation	8
3	Numerical results	11
	$3.1 m_{t\bar{t}} \text{ distributions}$	12
	3.2 Discrimination between $A \to ZH$ and $H \to ZA$	12
4	Summary and conclusions	15

1 Introduction

A Impact of box-diagram contribution

B Impact of smearing top-quark momenta on c_{hel} and c_{han}

Contents

In 2012 the LHC discovered a Higgs boson which, at the current level of experimental precision, behaves in agreement with the predictions of the Standard Model (SM) [1, 2]. While the SM predicts only one Higgs boson, theories beyond the SM (BSM) often contain more than one fundamental spin-0 particle. Consequently, the search for additional Higgs bosons is one of the prime tasks of the current and future LHC programme.

Most searches for additional Higgs bosons focus on the production of one BSM resonance. However, BSM theories that contain additional Higgs fields that are charged under the electroweak (EW) gauge symmetry predict more than one BSM Higgs boson. Such BSM theories have the potential to resolve some of the most pressing open questions that remain unanswered in the SM, e.g. extended Higgs sectors can provide an explanation of the observed matter-antimatter asymmetry via EW baryogenesis [3], and additional neutral scalar particles can be stable and account for the observed cosmological abundance of dark matter. Consequently, during Run 2 at 13 TeV, ATLAS and CMS also performed searches for signals in which two BSM spin-0 resonances are involved. These searches mostly comprise signatures with a heavy BSM resonance decaying into a lighter BSM resonance and either a 125 GeV Higgs boson or a massive gauge boson [4].

Among these, searches for a neutral spin-0 particle decaying into another neutral spin-0 particle and a Z-boson have gathered significant attention [5–9]. This search channel has been identified as a "smoking-gun" signature for a first-order EW phase transition in the Two Higgs doublet model (2HDM) [7, 9–11]. A sufficiently strong EW phase transition is a required ingredient for the realisation of EW baryogenesis [3, 12–14], and it leads to the

production of a primordial gravitational-wave background that might be in reach of future space-based gravitational-wave detectors [7, 15, 16].

Assuming CP conservation, the 2HDM predicts a second CP-even Higgs boson H and a CP-odd Higgs boson A. A strong EW phase transition typically requires a sizeable mass splitting between these two states [11], and (depending on their mass hierarchy) either the decay $H \to ZA$ or the decay $A \to ZH$ can be kinematically allowed. Furthermore, since the top quark has the largest Yukawa coupling, its interactions are well-suited for providing the CP-violating source term that generates the baryon asymmetry. As a consequence, small values of $\tan \beta$ are preferred for EW baryogenesis [17], and the dominant decay modes for the lighter resonance in the 2HDM are $A/H \to t\bar{t}$ if its mass exceeds the di-top threshold, giving rise to $Zt\bar{t}$ final states. Notably, parameter points facilitating the decay $A \to ZH$ are more favourable for a successfully realisation of EW baryogenesis compared to the ones featuring the $H \to ZA$ decay [10, 14, 18–20]. It will therefore be crucial to be able to experimentally distinguish between the two decay modes if a signal in the "smoking gun" searches will be observed at the LHC in the future.

Searches for this signal in $Zt\bar{t}$ final states have been recently performed for the first time by both ATLAS and CMS, using the Run 2 data collected at 13 TeV [21, 22]. The resulting experimental limits have been exploited in ref. [9] by demonstrating that they exclude substantial parts of the 2HDM parameter space giving rise to a strong first-order EW phase transition. In both the ATLAS and the CMS analyses, the applied experimental analyses lack sensitivity to the CP-properties of the BSM particles. Therefore, a distinction between the $A \to ZH$ and the $H \to ZA$ signatures is not possible if both signals predict the same total cross section. In this work, we propose to use angular variables in $Zt\bar{t}$ final states in order to distinguish between $A \to ZH$ and $H \to ZA$ signals where the lighter BSM particle decays into a pair of top quarks, which subsequently decay leptonically.

Our study demonstrates that sensitivity to the CP-properties of the BSM particles can be achieved by exploiting the dependence of the $t\bar{t}$ invariant mass distribution $(m_{t\bar{t}})$ on angular variables defined in terms of the direction of flight of the leptons produced in the leptonic decay of the top quarks.¹ By considering the angular correlations of the leptons, we show that distinguishing between the two signatures is feasible with the anticipated 3000/fb of data collected during the high-luminosity phase of the LHC, even if they possess the same total cross section. It is worth noting that the relevant angular variables have been previously employed in searches for a single new particle decaying into top-quark pairs at both the Tevatron [24] and the LHC [25–27], see also ref. [28]. We demonstrate here the potential of extending such an experimental strategy based on angular variables to signatures involving two BSM particles.

In addition to obtaining a discrimination power between the two potential signals, we demonstrate that a refined analysis technique utilizing angular variables also improves the signal-background discrimination, and thus the overall experimental sensitivity. Here it should be noted that our approach relies on the leptonic decays of both top quarks, in contrast to the experimental analyses conducted by ATLAS [21] and CMS [22], which only

 $^{^{1}}$ An analysis of the CP properties of a BSM resonance decaying into a Z boson and the 125 GeV Higgs boson, the latter assumed to be purely CP even, can be found in ref. [23].

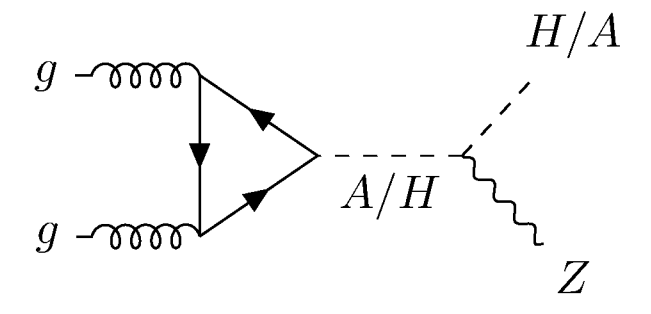


Figure 1. Feynman diagram of the considered signals with H and A being a CP-even and a CP-odd spin-0 resonance, respectively.

incorporate the semi-leptonic and the fully hadronic decays, respectively. As a result, while there exists potential for increased background rejection, this potential of our proposed analysis comes at the cost of a reduced number of signal events resulting from the requirement of leptonically decaying top quarks. On the other hand, the angular information obtained from the leptons in the signal regions where both top quarks decay leptonically can be combined with the experimental information gained from the signal regions targeting semileptonically and hadronically decaying $t\bar{t}$ pairs for which our approach is not directly applicable.²

The outline of our paper is as follows. In section 2 we introduce the theoretical framework, including a brief description of the 2HDM that we use as a theoretical framework in order to benchmark our results, and a detailed discussion of the Monte Carlo simulation of the considered process. In particular, we discuss the implementation of the angular variables in the experimental analysis that are sensitive to the spin correlations of the top-quark pairs. In section 3 we present the results of our simulation, focusing on the one hand on the discrimination between the signals and the SM background, and on the other hand on the discrimination between the two potential signals. We summarise our results and conclude in section 4.

2 Theoretical framework and simulation

In order to demonstrate the application of the angular variables to the $m_{t\bar{t}}$ distribution in the processes $A \to ZH \to Zt\bar{t}$ and $H \to ZA \to Zt\bar{t}$, we perform a Monte-Carlo (MC) simulation of both signals and SM background. The Feynman diagram for the production of the two signals is depicted in figure 1. For our simulations we choose the 2HDM as theoretical framework, noting that our conclusions can be applied more generally to any BSM theory with an extended scalar sector featuring at least two neutral extra Higgs bosons with opposite CP charges (or potentially two CP-mixed states for the case of CP violation) such that a coupling of the form AHZ is present.

²The measurement of $t\bar{t}$ spin correlations may also be feasible in the semileptonic channel with the data collected during the high-luminosity phase of the LHC [29, 30], relying on the possibility of charm-tagging [31]. However, we focus here on the fully leptonic channel since it is the final state with the highest sensitivity to the $t\bar{t}$ spin information, see the discussion in section 2.2.

	$BP_{H\to ZA}$	$BP_{A \to ZH}$
$\tan \beta$	1.14	1.50
$\cos(\beta - \alpha)$	0	0
$m_h/{ m GeV}$	125	125
$m_H/{ m GeV}$	800	600
$m_A/{ m GeV}$	600	800
$m_{H^\pm}/{\rm GeV}$	800	800
$M/{ m GeV}$	600	600
$BR(H \to t\bar{t})$	71%	99%
$\mathrm{BR}(A \to t \bar{t})$	99%	63%
$BR(H \to ZA)$	29%	_
$\mathrm{BR}(A \to ZH)$	_	37%
Γ_H/m_H	4.3%	1.5%
Γ_A/m_A	3.5%	3.3%
$\sigma(gg \to H)/\mathrm{pb}$	0.35	0.89
$\sigma(gg \to A)/\mathrm{pb}$	2.43	0.27

Table 1. Definitions of the benchmark points $BP_{H\to ZA}$ and $BP_{A\to ZH}$ and predicted branching ratios, total widths and gluon-fusion production cross sections at the LHC with $\sqrt{s} = 13$ TeV.

2.1 The 2HDM

The 2HDM [32] augments the scalar sector of the SM by a second scalar SU(2) doublet field. For the case of CP conservation, the 2HDM predicts two CP-even Higgs bosons h and H, one CP-odd Higgs boson A, and a pair of charged Higgs bosons H^{\pm} . The angles α and β diagonalise the CP-even and CP-odd scalar sectors of the model, respectively. In addition, $t_{\beta} \equiv \tan \beta$ is given by the ratio of the two Higgs doublet vacuum expectation values. Throughout this work, the lighter CP-even Higgs boson h corresponds to the detected Higgs boson at 125 GeV. Parameter space regions that give rise to EW baryogenesis favour small values of t_{β} (see the discussion above) and the alignment limit (defined by $\cos(\beta - \alpha) = 0$), in which h resembles the Higgs boson predicted by the SM, as well as a sizeable mass splitting between the pseudoscalar A and the second CP-even scalar H.

Our analysis targets signal cross sections that are compatible with the limits from the LHC searches performed during Run 2, but which lie in reach of the high-luminosity LHC (HL-LHC) with an anticipated integrated luminosity of 3000/fb. For ease of comparison we use a centre-of-mass energy of $\sqrt{s}=13\,\mathrm{TeV}$ also for the HL-LHC. As a representative 2HDM benchmark point we choose masses of 600 GeV for the lighter and 800 GeV for the heavier BSM resonance, respectively. The mass of the charged Higgs bosons is set to be equal to the mass of the heavier BSM state, $m_{H^\pm}=800\,\mathrm{GeV}$, to satisfy constraints from electroweak precision observables [33]. We also assume the alignment limit, i.e. $\cos(\beta-\alpha)=0$. Regarding t_β , we use two different values depending on the mass hierarchies of H and A in order to predict the same total cross

section for the two possible signals. We use a value of $t_{\beta} = 1.5$ for the case $m_A = 800 \,\text{GeV}$ and $m_H = 600 \,\text{GeV}$, and $t_{\beta} = 1.14$ for the case $m_H = 800 \,\text{GeV}$ and $m_A = 600 \,\text{GeV}$, such that for both signals we find $\sigma[pp \to A(H) \to Z\,H(A) \to Z\,t\bar{t}] = 0.1$ pb. Here the production cross sections of H and A were computed at NNLO in QCD using HiggsTools [34] (see also the discussion in section 2.3.2), and their branching ratios were computed using HDECAY [35, 36], including state-of-the-art QCD corrections. The remaining 2HDM parameter m_{12}^2 is not relevant for the considered signature. To fix m_{12}^2 , in our analysis we set the BSM mass scale $M^2 = m_{12}^2/(\sin\beta\cos\beta)$ equal to the mass of the lighter BSM Higgs boson, $M = 600 \,\text{GeV}$, in order to comply with theoretical constraints from vacuum stability [37, 38] and perturbative unitarity [39] which we checked using THDMTOOLS [9]. The values of the free parameters for the two considered benchmark scenarios are summarised in table 1, where we also show the relevant branching ratios, the total widths and the cross sections of the neutral BSM scalars.

Using the HiggsBounds [40–43] module contained in HiggsTools [34], we verified that the two benchmark points pass the LHC cross section limits from searches for $H^{\pm} \to tb$ [44, 45] and from searches for $A/H \to t\bar{t}$ in $t\bar{t}t\bar{t}$ final states [46, 47]. The benchmark points are also compatible with the limits on $Ht\bar{t}$ and $At\bar{t}$ couplings from searches for $A/H \to t\bar{t}$ in the di-top final state obtained by CMS utilising the first-year Run 2 data [25]. Recently, both ATLAS [26] and CMS [27] reported preliminary results of searches in the di-top final state including the full Run 2 dataset. Due to the large interference effects between the signal and the QCD background the resulting limits depend on the width of the new particle. No limits are presented for a relative width of about 3.5% that we find for the lighter resonance in our benchmark points, see table 1. Assuming that the limits given for a relative width of 5\% are approximately applicable to our benchmark points, the limits from the new searches would be in tension with our benchmark points at about the 2σ level. However, since we are mainly interested in the improvement of the searches in the $Zt\bar{t}$ final state that can be achieved by exploiting top-quark spin correlations, and not in a comparison between searches in different final states, we stick to our benchmark points. We also stress that the cross sections for the $gg \to A \to ZH$ and $gg \to H \to ZA$ signals decrease more slowly with increasing t_{β} compared to the direct production of the lighter state $gg \to H$ and $gg \to A$, respectively, see the discussion below. Hence, for t_{β} values larger than the ones considered in our benchmark points, the lighter state could be detected first via its production from the decay of a heavier BSM resonance as in the channel investigated here rather than via its direct production and searches using the $t\bar{t}$ final state [9].

We show in figure 2 the total cross sections for the heavier BSM resonance (top), the branching ratios for the $A \to ZH$ and $H \to ZA$ decays (middle), and the total signal cross section contributing to $Zt\bar{t}$ production (bottom) as a function of t_{β} , with all other parameters fixed as shown in table 1. The gluon fusion production is dominated by the contribution from the top-quark loop. Since the absolute values of the couplings of H and A to the top quark scale with a factor of $1/t_{\beta}$, the cross sections shown in the top plot are approximately proportional to $1/t_{\beta}^2$. The decrease of the production cross section of the heavier BSM resonance with increasing values of t_{β} is partially compensated by an increase of BR $(A \to ZH)$ and BR $(H \to ZA)$ with increasing value of t_{β} , as shown in the plot in the middle. In both benchmark scenarios, the lighter BSM resonance dominantly decays via $H/A \to t\bar{t}$ with a branching ratio of more than 99% for the small values of t_{β} relevant here.

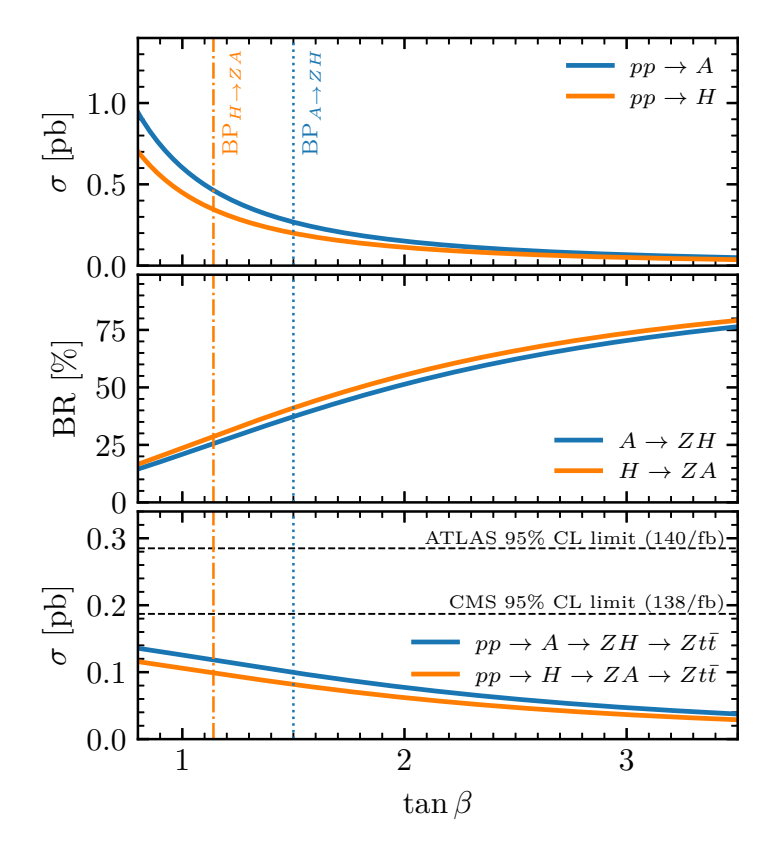


Figure 2. Top: gluon-fusion production cross section at 13 TeV for the heavier BSM spin-0 resonance (with a mass of 800 GeV) as a function of t_{β} . Centre: branching ratios for the heavy spin-0 resonance decaying into the lighter spin-0 resonance (with a mass of 600 GeV) and a Z-boson as a function of t_{β} . Bottom: signal cross sections contributing to $Zt\bar{t}$ production as a function of t_{β} . The horizontal black dashed lines show the current experimental 95% CL limits from ATLAS [21] and CMS [22] using an integrated luminosity of 140/fb and 138/fb, respectively. In all plots the orange and blue vertical lines correspond to the benchmark points $BP_{H\to ZA}$ and $BP_{A\to ZH}$, respectively, which are defined in table 1.

As a consequence, the final signal cross sections show an approximately linear dependence on $1/t_{\beta}$, as is visible in the bottom plot, where we also indicate with the horizontal black dashed lines the current 95% CL cross-section limits found by ATLAS [21] and CMS [22] including 140/fb and 138/fb, respectively, collected during Run 2.

2.2 Angular variables

To gain information on the CP nature of the BSM resonances, we propose to utilize the spin correlations of the final state $t\bar{t}$ pair. The production density matrix of two top quarks can be written in terms of the Pauli matrices σ as [48]

$$R \propto A \, \mathbb{1} \otimes \mathbb{1} + B_i^+ \sigma^i \otimes \mathbb{1} + B_i^- \mathbb{1} \otimes \sigma^i + C_{ij} \sigma^i \otimes \sigma^j \,, \tag{2.1}$$

where A and the vector \vec{B}^{\pm} arise from the parton level kinematics and the polarisations of the di-top state, respectively. The spin correlations of the top and anti-top quarks are encoded in the matrix C. They are commonly extracted experimentally by evaluating observables in an

orthonormal basis $(\hat{k}, \hat{r}, \hat{n})$. The coordinate \hat{k} is defined as the unit vector of the top-quark direction in the zero-momentum frame (ZMF), which is equal to the centre-of-mass frame of the $t\bar{t}$ system. Taking \hat{p} as the direction of flight of one of the incoming protons, the scattering angle of the top quark is given by $\cos \theta_t = \hat{p} \cdot \hat{k}$, which can be used to obtain the unit vector

$$\hat{n} = \frac{\operatorname{sign}(\cos \theta_t)}{\sin \theta_t} (\hat{p} \times \hat{k}). \tag{2.2}$$

We define the remaining coordinate as $\hat{r} = -\hat{n} \times \hat{k}$. Assuming fully leptonic decays of both top quarks, the leptons are boosted first to the di-top ZMF frame and subsequently to their respective parent top-quark ZMF. Their directions of flight are denoted as $\hat{\ell}^+$ and $\hat{\ell}^-$. The normalised angular distributions can then be written in terms of \vec{B}^{\pm} and C as

$$\frac{1}{\sigma} \frac{d\sigma}{d\Omega^+ d\Omega^-} = \frac{1}{(4\pi)^2} (1 + \kappa_\ell \vec{B}^+ \cdot \hat{\ell}^+ + \kappa_\ell \vec{B}^- \cdot \hat{\ell}^- - \kappa_\ell^2 \hat{\ell}^+ \cdot C \cdot \hat{\ell}^-)$$
 (2.3)

for solid angles $d\Omega^{\pm}$. We assume a spin analysing power of $\kappa_{\ell} = 1$ for leptons, which is the case at tree-level (higher orders effects are of relative order 10^{-3} [49] or smaller). Quarks have spin analysing powers smaller than unity and receive larger corrections from higher QCD orders, rendering the fully-leptonic channel the easiest case for extracting the top-quark spin-correlations [50].

Choosing a reference axis $\hat{a} \in \{\hat{k}, \hat{r}, \hat{n}\}$, the angle of the lepton and the axis is given by $\cos \theta_{\hat{a}}^{\pm} = \pm \hat{\ell}^{\pm} \cdot \hat{a}$. Allowing for different axes $\hat{a}, \hat{b} \in \{\hat{k}, \hat{r}, \hat{n}\}$, the differential cross section for a choice of axes after integrating over azimuthal angles is then given by

$$\frac{1}{\sigma} \frac{d\sigma}{d\cos\theta_{\hat{a}}^{+} d\cos\theta_{\hat{b}}^{+}} = \frac{1}{4} (1 + B_{\hat{a}}^{+} \cos\theta_{\hat{a}}^{+} + B_{\hat{a}}^{-} \cos\theta_{\hat{a}}^{-} - C_{\hat{a}\hat{b}} \cos\theta_{\hat{a}}^{+} \cos\theta_{\hat{b}}^{-}), \qquad (2.4)$$

where we have written the vectors \vec{B}^{\pm} and the matrix C in terms of their components. The connection of $\cos \theta_{\hat{a}}^{+} \cos \theta_{\hat{b}}^{-}$ to the spin correlations of the $t\bar{t}$ system renders them well-suited observables to distinguish between cases of different parities. This can be employed for example (as considered here) to distinguish whether the top-quark pair originated from a scalar or pseudoscalar state. Similarly to refs. [27, 51–53] we use the observables

$$c_{hel} = -\cos\theta_{\hat{k}}^{+}\cos\theta_{\hat{k}}^{-} - \cos\theta_{\hat{r}}^{+}\cos\theta_{\hat{r}}^{-} - \cos\theta_{\hat{n}}^{+}\cos\theta_{\hat{n}}^{-},$$

$$c_{han} = \cos\theta_{\hat{k}}^{+}\cos\theta_{\hat{k}}^{-} - \cos\theta_{\hat{r}}^{+}\cos\theta_{\hat{r}}^{-} - \cos\theta_{\hat{n}}^{+}\cos\theta_{\hat{n}}^{-},$$

$$(2.5)$$

which are sensitive to the CP-nature of the state producing the top-quark pair.³ The diagonal spin correlation coefficients that contribute to the c_{hel} and c_{han} observables have been studied for the $t\bar{t}Z$ channel in ref. [54]. They obtain different values compared to the $t\bar{t}$ channel (without an emitted Z boson) for the SM. Most importantly, in $t\bar{t}Z$ the diagonal spin correlation coefficients have the opposite sign compared to $t\bar{t}$ which implies that the same should be true for c_{hel} . We investigate this further including the effects from additional (pseudo)scalars in sections 2.3.1 and 2.3.2.

³The parameter c_{hel} is called D in ref. [51], and c_{han} is called D_3 in ref. [52].

2.3 Monte Carlo simulation

To study the impact on the c_{hel} and c_{han} observables from additional scalar states in the $t\bar{t}Z$ channel, we perform a numerical MC simulation using MADGRAPH5_AMC@NLO [55, 56]. We use FeynRules [57, 58] to extend the SM model with the additional interactions of interest that couple the scalar and pseudoscalar to the top quark and the Z boson,

$$\mathcal{L} \supset -\frac{m_t}{vt_{\beta}}\bar{t}(H + iA\gamma_5)t - \frac{e}{2s_W c_W}(H\partial_{\mu}A - A\partial_{\mu}H)Z^{\mu}, \qquad (2.6)$$

where s_W , c_W denote the sine and cosine of the weak mixing angle, $v \approx 246 \,\text{GeV}$ is the SM Higgs vacuum expectation value, and e is the electric charge. The effective interactions between the (pseudo)scalar and the gluon field are also introduced,

$$\mathcal{L} \supset \frac{\alpha_S}{8\pi v} \left[\mathcal{F}_H(\tau) H G^a_{\mu\nu} G^{a\mu\nu} + i \mathcal{F}_A(\tau) A G^a_{\mu\nu} \tilde{G}^{a\mu\nu} \right] , \qquad (2.7)$$

where the strong coupling constant is denoted by α_S . The interactions are exported as a UFO [59, 60] model file with an additional pseudoscalar A and scalar H. The UFO file is extended to include the momentum-dependent form factors arising from the top-quark triangle loop [61]

$$\mathcal{F}_H(\tau) = \frac{1}{\tau^2} \left(\tau + (\tau - 1) f(\tau) \right) ,$$
 (2.8)

$$\mathcal{F}_A(\tau) = -\frac{1}{\tau} f(\tau) , \qquad (2.9)$$

where $\tau = \hat{s}/(4m_t^2)$. The function $f(\tau)$ is given by

$$f(\tau) = \begin{cases} \arcsin^2(\sqrt{\tau}) & \tau \le 1, \\ -\frac{1}{4} \left[\log \frac{1+\sqrt{1-\tau^{-1}}}{1-\sqrt{1-\tau^{-1}}} - i\pi \right]^2 & \tau > 1. \end{cases}$$
 (2.10)

We have cross-checked our matching of the effective vertex to the triangle loop contribution using FeynArts [62, 63] and FormCalc [64].

2.3.1 Background

In the fully leptonic channel, the main background is the SM $pp \to t\bar{t}Z$ production from proton collisions which we simulate at leading order with leptonic decays of the top quarks, $t \to b\ell\nu_\ell$, and $Z \to \ell^+\ell^-$. By extracting the c_{hel} and c_{han} observables, we show the two-dimensional differential distribution in the left plot of figure 3 in arbitrary units (a.u.), defined as the number of events in each bin divided by the total number of events. For comparison we additionally show in the middle plot the SM distribution of $pp \to t\bar{t}$ with leptonic decays that shows the opposite behaviour, as expected from the discussion in section 2.2, due to the opposite signs of the diagonal elements of the spin-correlation matrix [54]. It should be noted that the differences in these distributions can be attributed to the emission of a spin-one particle. Unlike $t\bar{t}Z$, the emission of a spin-zero boson, such as the Higgs boson, does not induce the same effect. For comparison, the distribution for $t\bar{t}h$ production is also shown in the right plot of figure 3, which has the same overall shape as the $t\bar{t}$ distribution.

 $^{^4}$ We discuss the background rate normalisation in section 3.

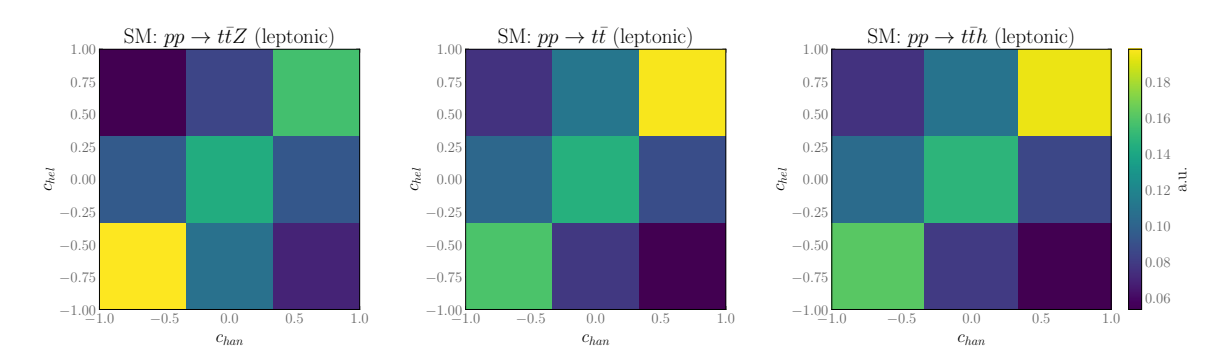


Figure 3. Two-dimensional distributions in the c_{hel} - c_{han} plane for different SM channels. Our process of interest $t\bar{t}Z$ (left) has a c_{hel} value with opposite sign compared to $t\bar{t}$ (middle) and $t\bar{t}h$ (right).

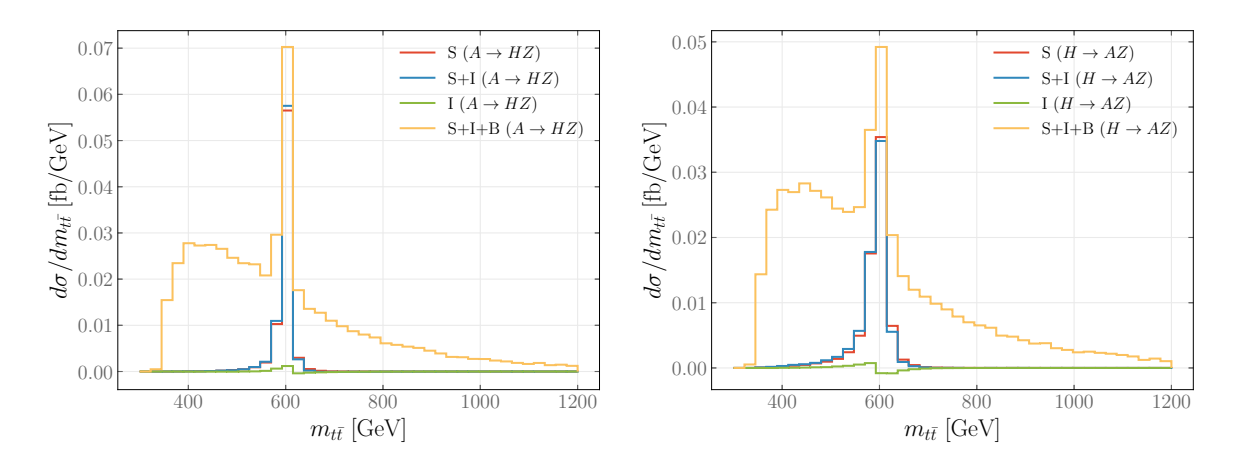


Figure 4. Histograms for the $m_{t\bar{t}}$ invariant mass distribution for the $A \to HZ$ (left) and the $H \to AZ$ process (right). The pure-signal and pure-background contributions are indicated with S and B, respectively, while I denotes the signal-background interference at leading order.

2.3.2 Signal

The signal processes under consideration are

$$gg \to \begin{pmatrix} A \\ H \end{pmatrix} \to \begin{pmatrix} ZH \\ ZA \end{pmatrix} \to Z t \bar{t} \to \ell^+ \ell^- b \bar{b} \ell^+ \ell^- \nu_\ell \bar{\nu}_\ell$$
 (2.11)

where we focus in particular on the distinction between the $A \to HZ$ and $H \to AZ$ signals. The cross sections are corrected by calculating K-factors as the ratio of the QCD next-to-next-to-leading order $gg \to A/H$ production cross sections obtained with the HiggsTools framework [34], which incorporates predictions obtained with SusHi [65, 66], divided by the leading-order $gg \to A/H$ production cross sections obtained with MAD-GRAPH5_AMC@NLO.⁵ As discussed above, for the two benchmark scenarios defined in section 2.1 the two signal processes $gg \to A \to ZH$ and $gg \to H \to ZA$ have the same total cross section. This makes them indistinguishable in the searches recently performed

⁵The K-factor for the pseudoscalar is 2.04, while for the scalar it is 2.08 using a fixed renormalisation scale in MadGraph5_aMC@NLO.

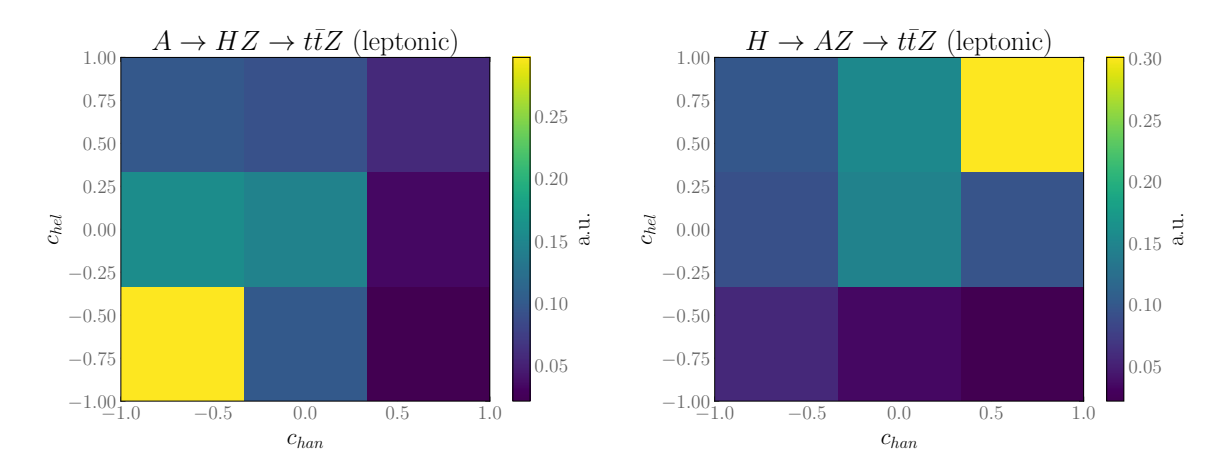


Figure 5. Two-dimensional distributions for c_{hel} and c_{han} for the $A \to HZ$ and $H \to AZ$ channels, indicating the potential power to discriminate the two signatures if the two observables are utilised in the $t\bar{t}Z$ final state.

by ATLAS and CMS, where the fully leptonic channel and the angular information of the final-state leptons have not been exploited.

We include interference effects between the signal and the SM $gg \to t\bar{t}Z$ background and calculate the c_{hel} and c_{han} observables after subtracting the SM background. In particular, differential distributions for the $gg \to t\bar{t}Z$ channel (including the decays of the top quarks) are obtained by calculating the full result for the distribution consisting of the BSM, SM and interference contributions $d\sigma_{\rm full}$ and subtracting the pure-SM contribution, i.e. $d\sigma_{\rm BSM} = d\sigma_{\rm full} - d\sigma_{\rm SM}$. The interference effects are in general small as shown in figure 4, where the invariant $m_{t\bar{t}}$ distribution for the $A \to ZH$ channel is displayed on the left and for the $H \to ZA$ channel on the right.

We do not include additional interference contributions between $gg \to A/H \to (H/A)Z$ and box diagrams resulting in the same final states, $gg \to (H/A)Z$ (an example diagram is shown in figure 10 below). We have checked their importance at the $t\bar{t}Z$ parton level (not including the decays of the top quarks) with a loop-ready model file produced with NLOCT [67] and found that the impact of the box-diagrams is negligible, see appendix A.

The differential cross section distributions in terms of c_{han} and c_{hel} (in a.u.) for the two signals $A \to HZ$ and $H \to AZ$ are shown in figure 5 (the range of the colour coding is different than in figure 3). The displayed results show that the c_{hel} and c_{han} variables can potentially provide sensitivity for distinguishing the two signals. While the $A \to HZ$ signal peaks for negative c_{hel} and c_{han} , the $H \to AZ$ signal peaks for positive c_{hel} and c_{han} . Furthermore, unlike the SM distributions, the $A \to HZ$ and $H \to AZ$ signal distributions are not only concentrated in the diagonal bins. Thus, exploiting the variables c_{hel} and c_{han} and their interplay appears to be a promising approach towards a possible distinction between the two signals in a realistic analysis.

⁶In practice we achieve this by modifying the matrix element in MadGraph5_aMC@NLO in order to improve numerical stability.

3 Numerical results

We proceed to examine the statistical significance of the two considered signals, $A \to HZ$ and $H \to AZ$, through an analysis utilising the c_{hel} and c_{han} observables as well as the invariant mass of the di-top state, $m_{t\bar{t}}$. We design our phenomenological analysis following the approach of ATLAS for the differential cross section measurements of $t\bar{t}Z$ production [68]. For simplicity we work with parton-level events, but set requirements for the signal region similar to the ATLAS experiment and subsequently apply Gaussian smearing (see the discussion in ref. [28]). Selected leptons are required to have a transverse momentum $p_T(\ell) > 10 \,\text{GeV}$ and pseudorapidity $|\eta(\ell)| < 2.5$. At least two pairs of opposite-sign same-flavour leptons must be identified, where the leading lepton needs to have a p_T value exceeding 27 GeV. One lepton pair must have an invariant mass close to the mass of the Z boson, $|m_Z - m_{\ell\ell}| < 20 \,\text{GeV}$. We require at least two jets with $p_T(j) > 25 \,\text{GeV}$ and $|\eta(j)| < 2.5$, as b-quarks can only be tagged in the central part of the detector. The parton-level top quarks and their daughter leptons are identified from MC-truth information saved in the LHE [69] files. In an actual experimental analysis, the four-momenta of the two top-quarks are reconstructed using the four-momenta of the daughter leptons. The proper reconstruction of the $t\bar{t}$ -system with fully leptonic decays is non-trivial due to the undetected neutrinos, and relies on algebraic kinematic reconstruction methods by imposing p_T conservation and the masses of the W-bosons and top-quarks as constraints [70–72]. The reconstruction efficiency using this technique has been shown to be about 94% in the tt channel [72]. For the ttZ final state, the presence of the leptonically decaying Z boson does not hamper the reconstruction efficiency of the top-quark pair, as its invariant mass can be identified from a reconstructed $\ell^+\ell^-$ pair. Moreover, we verified that a smearing on the momenta of the top and anti-top quarks to account for finite detector resolution effects on the reconstruction has no significant impact on the c_{hel} and c_{han} distributions, see appendix B. We therefore regard it as sufficient to consider a smearing on the $m_{t\bar{t}}$ distribution in our analysis.

ATLAS [68] expects about 101 events from the SM $t\bar{t}Z$ channel, while the total number of expected events including additional backgrounds rises to 139 (the sum of background events in the SR-4 ℓ -SF and SR-4 ℓ -DF signal regions) for an integrated luminosity of 140/fb. We choose to normalise our background sample such that we obtain 139 events at the same integrated luminosity (we use MADGRAPH5_AMC@NLO to obtain the shape of the background distributions, assuming that it follows the main $t\bar{t}Z$ background).

Apart from the K-factors applied to both of the signals, as discussed in section 2.3.2, we additionally apply efficiency factors that equally reduce the cross section rates for $A \to HZ$ and $H \to AZ$. We apply an efficiency factor of $(0.7)^2$ for b-tagging and a factor of 0.9 for correctly identifying the reconstructed top quarks and their daughter leptons [71, 72].

Throughout this section we will evaluate the statistical significance of the $A \to HZ$ and $H \to AZ$ signals w.r.t. the SM in each bin i with

$$Z_i = \sqrt{2\left[\left(S_i + B_i\right)\log\left(1 + \frac{S_i}{B_i}\right) - S_i\right]},$$
(3.1)

⁷The ATLAS analysis only requires one tagged *b*-jet [68].

where S_i and B_i denote the signal and SM background events in bin i, respectively [73]. Combined significances are subsequently obtained by summing in quadrature $Z = \sqrt{\sum_i Z_i^2}$ (without including bin-by-bin correlations). It should be noted that we do not include systematic uncertainties beyond efficiency factors for b-tagging and top-quark reconstruction, and therefore a real experimental analysis is expected to yield smaller significances than the ones obtained in our numerical analysis, see also the discussion below. Nevertheless, our evaluation of the significances will be useful in order to quantify the improvement of the experimental sensitivity as a consequence of incorporating the information from $t\bar{t}$ spin correlations.

$3.1 \quad m_{tar{t}} \; { m distributions}$

We first investigate the $m_{t\bar{t}}$ distributions from the $A\to HZ$ channel for a parameter point with $m_A=650\,\mathrm{GeV}$ and $m_H=450\,\mathrm{GeV}$ with $\tan\beta=1$. This is motivated by the fact that ATLAS has observed a $2.85\,\sigma$ excess for these mass values, compatible with this $\tan\beta$ value, in their search based on the full Run 2 data set in the semi-leptonic top-quark decay channel [21]. Using bins of 50 GeV and assuming a 20% Gaussian smearing to approximate detector effects, we evaluate the significance for each bin of the $m_{t\bar{t}}$ distribution. After summing in quadrature we obtain a combined significance of $3.8\,\sigma$ at $140/\mathrm{fb}$. While this significance is not directly comparable to the one obtained by ATLAS, as our phenomenological analysis has a different setup and uses a different channel, we regard the fact that the significance that we obtain for this example point is not far away from the ATLAS result as reassuring regarding the validity of our projections for the HL-LHC. The feature that our obtained significance is somewhat higher than the one found by ATLAS is expected since, as discussed above, we neglect systematic effects.

Subsequently, we proceed to study the $m_{t\bar{t}}$ distributions for $H\to AZ$ and $A\to HZ$ for the two benchmark scenarios defined in section 2.1 (as shown in figure 2 these parameter points are compatible with the current experimental limits from LHC searches in the $Zt\bar{t}$ final state). The expected events for the $m_{t\bar{t}}$ invariant mass distribution are shown in figure 6 for an integrated luminosity at the HL-LHC of 3/ab. We have assumed an improved smearing of 10% for the HL-LHC stage. As expected, the $m_{t\bar{t}}$ distribution does not yield any important differences between the scalar and the pseudoscalar production modes, implying that a resonance search utilising only $m_{t\bar{t}}$ would be unable to identify the CP properties of the resonance state. Evaluating the significances in each bin according to eq. (3.1) and combining the significances for the different bins yields a significance of 5.9 (5.5) for $A\to HZ$ ($H\to AZ$) with the assumed 10% smearing effect.

3.2 Discrimination between $A \to ZH$ and $H \to ZA$

We now incorporate information from $t\bar{t}$ spin correlations. As a first step we consider the case where either the angular observable c_{hel} or c_{han} is utilised. As a possible binning in c_{hel} , the generated events can be separated into the three different regions $c_{hel} < -0.33$, $-0.33 < c_{hel} < 0.33$ and $c_{hel} > 0.33$ such that separate results are obtained for the $m_{t\bar{t}}$ distributions in each region. For the case where c_{han} is utilised as single angular observable the same kind of binning can be chosen. Results for the two cases are shown in figure 7,

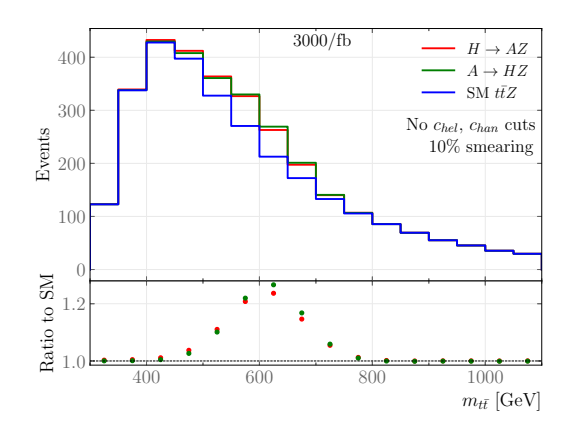


Figure 6. Expected events (upper plot) and ratio to the SM prediction (lower plot) for the di-top invariant mass distribution $m_{t\bar{t}}$ for an assumed integrated luminosity of 3/ab at the HL-LHC. The SM contribution to $t\bar{t}Z$ is shown in blue, while the $H \to AZ$ ($A \to HZ$) signals are shown in red (green).

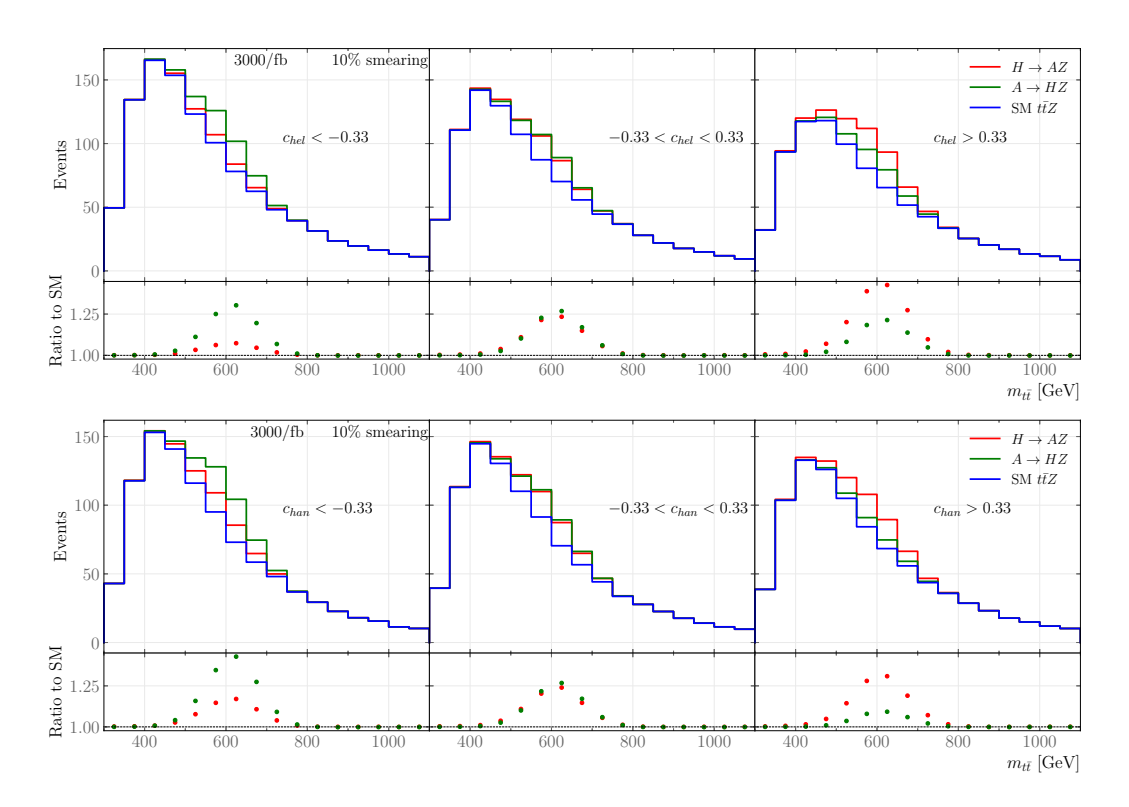


Figure 7. Expected events (upper plots) and ratio to the SM prediction (lower plots) for the di-top invariant mass distribution $m_{t\bar{t}}$ for different c_{hel} (top) and c_{han} (bottom) regions for an assumed integrated luminosity of 3/ab at the HL-LHC. The SM contribution to $t\bar{t}Z$ is shown in blue, while the $H \to AZ$ ($A \to HZ$) signals are shown in red (green).

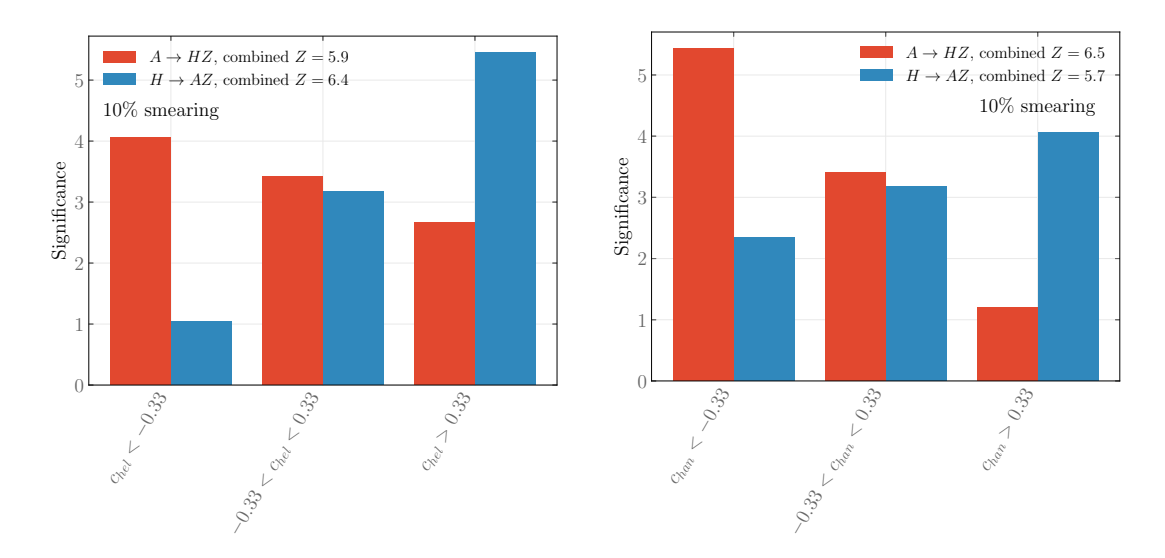
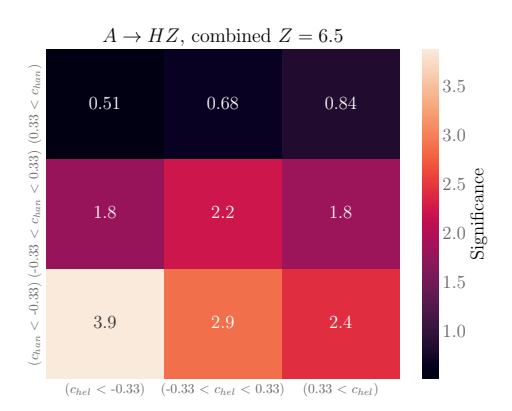


Figure 8. On the left, the significances that are obtained for the two signals are shown for the analysis splitting the events only according to the angular variable c_{hel} . On the right we show the significances for the analysis that utilises only the angular variable c_{han} .

where the expected $m_{t\bar{t}}$ distributions of the events and the ratio of the distributions including the $H\to AZ$ or $A\to HZ$ signals to the SM prediction are displayed for the different regions in c_{hel} or c_{han} for an integrated luminosity of 3/ab. The choice of using three regions for c_{hel} or c_{han} rather than a finer binning was made in order to ensure that the resulting $m_{t\bar{t}}$ bins are not depleted of background events. The $m_{t\bar{t}}$ binning of 50 GeV has been kept as for the case of section 3.1 where no angular variable is utilised. In line with the expectations from figure 5, for the case where c_{hel} is utilised as angular variable one observes a higher ratio of $A\to HZ$ events with respect to the SM for the $c_{hel}<-0.33$ region. In contrast, $H\to AZ$ yields a higher ratio w.r.t. the SM for $c_{hel}>0.33$. The highest value of the ratio across all regions is obtained for the $H\to AZ$ signal in this case. A similar pattern can also be observed for the c_{han} regions, albeit in this case the ratio to the SM across all the regions reaches higher values for $A\to HZ$. This indicates that c_{hel} and c_{han} have discriminating power allowing the separation between the $A\to HZ$ and $H\to AZ$ signals, in contrast to the case where one uses only the cross section rates or only the $m_{t\bar{t}}$ distribution.

In order to further quantify the sensitivity to the two signals, we evaluate the statistical significance in each $m_{t\bar{t}}$ distribution according to eq. (3.1) and then obtain the combined significance for each bin of the angular observable. The results are displayed in figure 8. We find that both cases, i.e. utilising only the angular variable c_{hel} or only the angular variable c_{han} , yield high significances for both signals $H \to AZ$ and $A \to HZ$. For the two cases the combined significances follow a similar pattern across the three bins of the angular variable. Furthermore, the two types of signals can be distinguished and thus, assuming that a potential signal consists of a CP eigenstate, the CP nature of this state can be determined. If in this case the highest significance is obtained from utilising a binning in c_{hel} and arises mostly from events with $c_{hel} > 0.33$, then evidently the signal is due to the production of a CP-even state, $gg \to H$. The opposite is true for a signal that originates from a CP-odd state, $gg \to A$, for which the highest significance would occur in the region $c_{han} < -0.33$.



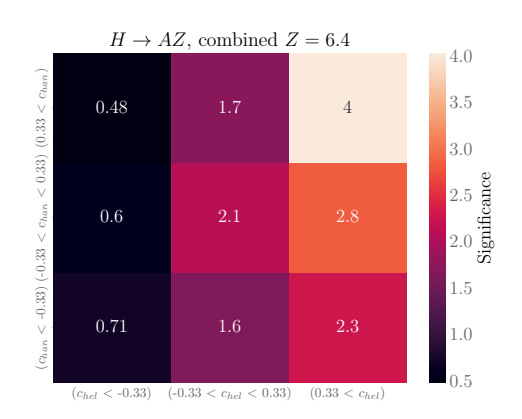


Figure 9. Significances for the approach where a simultaneous binning in both c_{hel} and c_{han} is utilised to define different regions. On the left we show the results for $A \to HZ$ and on the right for $H \to AZ$ for 3/ab with 10% smearing.

We furthermore note that utilising the angular observables has the potential to yield a higher significance compared to simply using the $m_{t\bar{t}}$ distribution. We find that the significance of the two signals does not surpass $6\,\sigma$ for the case where the spin-correlation observables are not taken into account. In contrast, binning in c_{hel} (c_{han}) gives rise to a significance of more than $6\,\sigma$ for the $H\to AZ$ ($A\to HZ$) signal, as shown in figure 8. We checked that this remains true even if one increases the number of bins in the $m_{t\bar{t}}$ distribution (we tried this for two cases by reducing the bin-size to 25 GeV and to 16.7 GeV). We note that this improvement of the significance of a detected signal will only occur in the data set where both top quarks decay leptonically, while signal regions based on semileptonically or hadronically decaying top-quark pairs will not be affected.

We now turn to the case where the two angular observables are exploited simultaneously. Thus, instead of only binning in either c_{hel} or c_{han} , we now use nine different regions arising from a simultaneous binning in both c_{hel} and c_{han} and construct $m_{t\bar{t}}$ distributions within each region. For this purpose we readjust the number of bins in the $m_{t\bar{t}}$ distribution to 80 GeV in order to avoid depleting any bin of background events and compute the combined significances in each region for the $H \to AZ$ and $A \to HZ$ signals. These results are shown in figure 9. We find similar conclusions to the case where only one of the angular observables is employed. The simultaneous binning in both observables yields a high sensitivity for distinguishing between the $A \to HZ$ and $H \to AZ$ signals, where the former is expected to have the highest significance in the $(c_{hel} < -0.33, c_{han} < -0.33)$ bin while the latter is expected to occur with the highest significance in the $(0.33 < c_{hel}, 0.33 < c_{han})$ bin. The overall significances for each of the two signals are found to be similar as for the case where only one of the angular observables is employed if the significances in the different regions are combined. Ultimately, the appropriate choice for the binning in the angular observables and the $m_{t\bar{t}}$ distribution will depend on the number of events that are obtained in the actual analysis at the HL-LHC.

4 Summary and conclusions

In this work, we have focused on (HL-)LHC searches for a new spin-0 boson, produced through gluon fusion, that decays into a Z boson and a lighter new spin-0 boson of opposite

CP character, where the latter decays into a pair of top quarks. Such a signal has been identified as a "smoking-gun" signature for a first-order EW phase transition in extended Higgs sectors like the Two Higgs doublet model (2HDM). In the absence of CP violation, the two spin-0 resonances involved in this process will be a CP-even state, H, and a CP-odd state, A, which can occur either as parent or daughter particle in the decay. Thus, the process can give rise to two possible signals, $gg \to A \to ZH \to Zt\bar{t}$ and $gg \to H \to ZA \to Zt\bar{t}$. The current experimental searches performed by ATLAS and CMS lack sensitivity to the CP properties of the spin-0 bosons. Therefore, these searches cannot distinguish between the two kinds of possible signals if the total production rates for the $Zt\bar{t}$ final state are predicted to be the same within the involved theoretical and experimental uncertainties.

We have proposed here a method to distinguish between the $A \to ZH$ and $H \to ZA$ signals that exploits the spin correlations of the $t\bar{t}$ system. To achieve this, we utilise the observables c_{han} and c_{hel} (defined in eq. (2.5)), which are reconstructed from the angular distributions of the two leptons produced in the fully leptonic decays of the two top quarks. These observables were previously applied in LHC searches for a single new resonance in the $t\bar{t}$ channel. We have demonstrated that the application of these angular observables can successfully be extended to signatures involving two BSM particles. In particular we have shown that exploiting the $t\bar{t}$ spin correlations is valuable in the $Zt\bar{t}$ channel both for determining the CP properties of new spin-0 resonances and to increase the overall experimental sensitivity.

We have used the CP-conserving 2HDM as a minimal UV-complete BSM framework that predicts two neutral BSM Higgs bosons H and A, which are CP-even and CP-odd, respectively. Therefore, our analysis then focuses on discriminating between the signals $H \to ZA$ and $A \to ZH$, which is phenomenologically of great interest since the presence of the latter is more favourable for a realisation of a strong first-order EW phase transition in the 2HDM. Such a phase transition is required for an explanation of the observed matter-antimatter asymmetry of the universe via EW baryogenesis, and it gives rise to a primordial gravitational-wave background that might be detectable with future space-based gravitational-wave experiments, such as LISA.

For our numerical analysis, we have defined two benchmark scenarios featuring a resonant $Zt\bar{t}$ production cross section of 0.1 pb and masses of 800 GeV and 600 GeV for the two Higgs bosons. While these rates are currently below the experimental sensitivity of the searches at the LHC in the $Zt\bar{t}$ channel, they are expected to be within the reach of the HL-LHC. In a first step, we have evaluated the statistical significance of the $A \to HZ \to t\bar{t}Z$ and $H \to AZ \to t\bar{t}Z$ signals from the cross section distributions w.r.t. the top-quark pair invariant mass, $m_{t\bar{t}}$. We have then explored the impact of considering the spin correlations from the di-top system by considering either a binning for one of the angular observables c_{hel} or c_{han} or a simultaneous binning for both of the angular observables.

Our results show that the signal $A \to HZ$ yields contributions to the angular observables that predominantly occur in the regions where c_{hel} and c_{han} are negative, while for $H \to AZ$ the largest contributions occur in the regions where both c_{hel} and c_{han} are positive. This behaviour allows one to infer information about the CP nature of the produced states, which is not possible with the current search strategy applied by ATLAS and CMS. In this way, a distinction between the two signals $A \to HZ$ and $H \to AZ$ is possible with high

statistical significance, which has important implications for assessing the possible realisation of EW baryogenesis and the prospects for a future detection of gravitational waves with observatories such as LISA.

It should be noted that the realisation of EW baryogenesis also requires new sources of CP violation. Therefore, in the future it would be worthwhile to investigate how precisely the CP properties of the produced new states could be determined if they are not CP eigenstates but a mixture of CP-even and CP-odd components. Such an analysis is beyond the scope of the present paper.

We have also shown that applying a binning of events with respect to either one of the angular variables (with an appropriate choice of c_{hel} or c_{han} for the two signals) or both of them yields a higher statistical significance for the signals compared to the SM background for both $A \to HZ$ and $H \to AZ$. For our chosen benchmark scenarios, we find an enhanced statistical significance of 6.4–6.5 for the case where the information from the angular variables c_{hel} and c_{han} is included, compared to 5.5–5.9 for the case where this information is not taken into account. Hence, the separation of events in different bins of c_{han} and c_{hel} is also promising for increasing the overall experimental sensitivity of the experimental searches, irrespective of whether the signature originates from the $A \to ZH$ or the $H \to ZA$ decay. It should be kept in mind, however, that our proposed analysis strategy is only directly applicable to the data set where both top quarks decay leptonically.

While the significances obtained in an actual experimental analysis may turn out to be somewhat smaller (due to systematic uncertainties not considered in our analysis) or larger (due to other systematic improvements in future CMS and/or ATLAS analyses) compared to our estimates, our results for the relative differences, which are the basis for demonstrating the discriminating power of our method, should provide reliable information about the potential of employing the spin correlation variables. In addition, since we have accounted for several sources of experimental uncertainties in our analysis, such as smearing of the $m_{t\bar{t}}$ distributions, our results should be unlikely to be significantly altered by detector effects.

In summary, we find that exploiting the information from top-quark spin correlations, through the observables c_{hel} and c_{han} , can provide crucial sensitivity to the CP properties of BSM states that are detectable in current and future $Zt\bar{t}$ searches at the (HL-)LHC, while the current searches carried out by ATLAS and CMS are insensitive to the CP nature of the produced states. We encourage the experimental collaborations to make use of this important source of information in their future Higgs-boson searches in the $Zt\bar{t}$ final state (and other $t\bar{t}+X$ final states) at the LHC by improving their search strategies along the lines that have been proposed in this paper.

Acknowledgments

We thank Matthias Schröder and Laurids Jeppe for helpful discussions. The project that gave rise to these results received the support of a fellowship from the "la Caixa" Foundation (ID 100010434). The fellowship code is LCF/BQ/PI24/12040018. T.B. acknowledges the support of the Spanish Agencia Estatal de Investigación through the grant "IFT Centro de Excelencia Severo Ochoa CEX2020-001007-S". F.A., P.S. and G.W. acknowledge support by the Deutsche Forschungsgemeinschaft (DFG, German Research Foundation) under Germany's

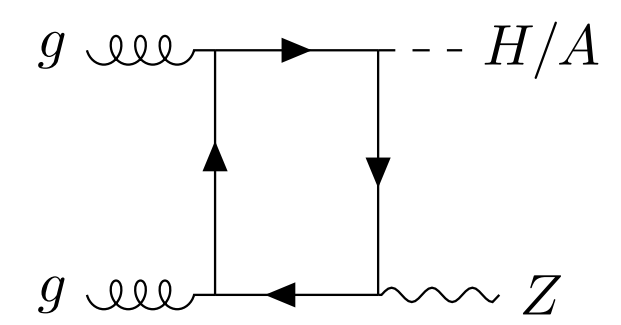


Figure 10. Box diagram resulting in the production of a scalar H or pseudoscalar A in association with a Z boson.

Excellence Strategy — EXC 2121 "Quantum Universe" — 390833306. The work of F.A., P.S. and G.W. has also been partially funded by the Deutsche Forschungsgemeinschaft (DFG, German Research Foundation) — 491245950.

A Impact of box-diagram contribution

The ZH and ZA final states considered here can also be produced via contributions involving a box-diagram. The corresponding type of Feynman diagram is depicted in figure 10. In order to assess the relevance of these contributions, we simulated events with MAD-GRAPH5_AMC@NLO including the box-diagrams at the $t\bar{t}Z$ parton level (not including the decays of the top quarks) with a loop-ready model file produced with NLOCT [67]. In figure 11 we show the cross section distributions for the $A \to ZH$ signal (left) and the $H \to ZA$ signal (right) as a function of the invariant mass of the top-quark pair (top row) and the invariant mass of the $t\bar{t}Z$ state (bottom row) for different contributions: the total signal (green), the interference between the resonant production and the box-diagram leading to HZ production (red), and the interference between the resonant production and the box-diagram leading to AZ production (blue). Overall, we find that the interference effects (blue and red lines) are small compared to the signal (green line). Our findings are in agreement with refs. [6, 21, 22]. We therefore do not take into account the production of a spin-0 resonance in association with a Z-boson via the box diagrams in our Monte-Carlo simulations.

B Impact of smearing top-quark momenta on c_{hel} and c_{han}

In experimental analyses, the need to reconstruct the top-quark momenta in final states involving neutrinos through algebraic reconstruction methods can lead to uncertainties in the components of the reconstructed momenta with respect to the actual momenta of the top quarks. This is not taken into account in our analysis since we use the MC-truth top-quark momenta and only apply a reconstruction efficiency to accommodate the case where top quarks could not be reconstructed. Here we investigate how sensitive the c_{hel} and c_{han} observables are to shifts of the components of the top-quark momenta caused by the finite detector resolution. To simulate detector effects, we perform a conservative 20% and 30% Gaussian smearing on the p_x, p_y, p_z components of the four-momenta for both the top and anti-top quarks and subsequently re-compute the c_{hel} and c_{han} variables for the events in our

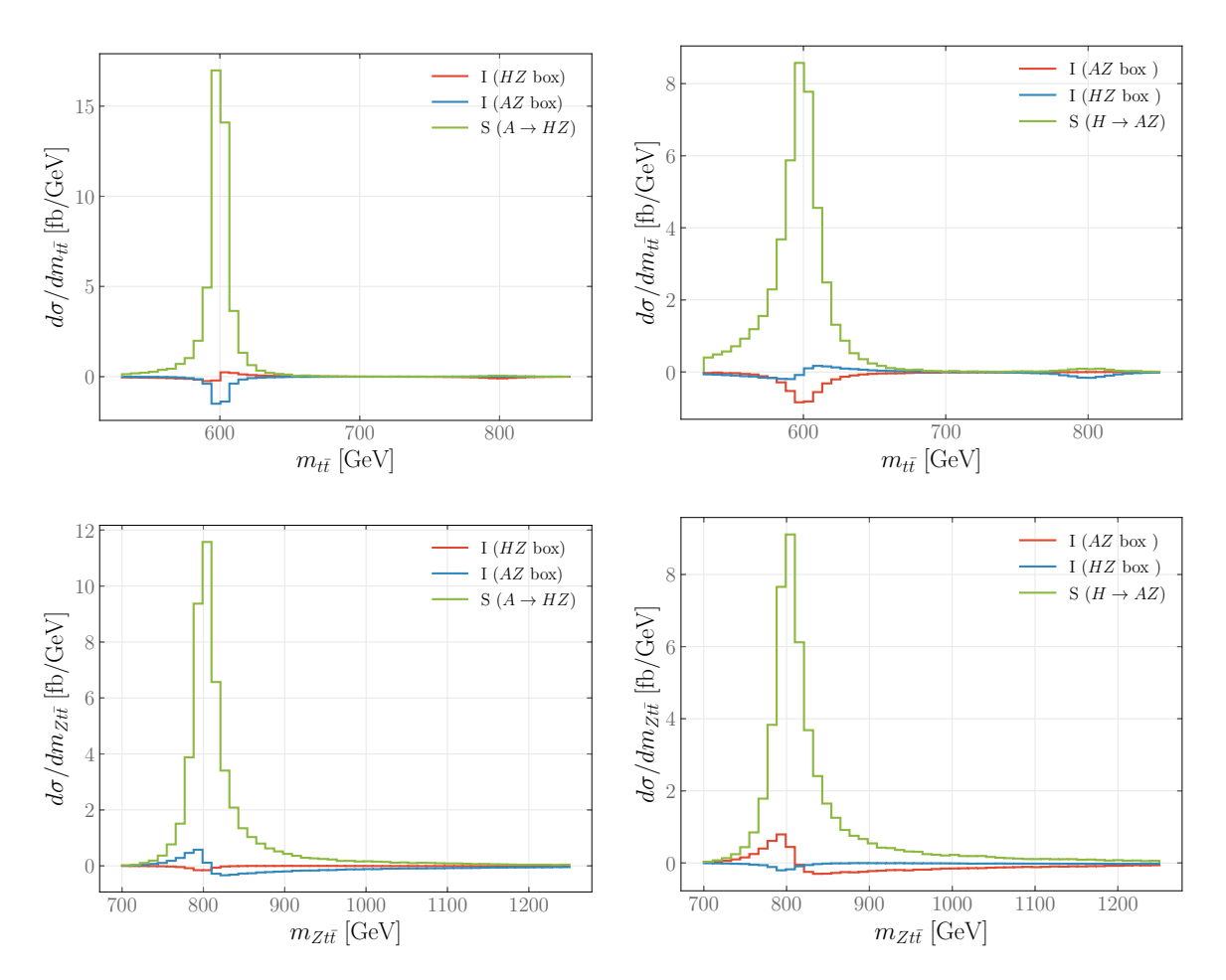


Figure 11. Distributions for the invariant mass of the top-quark pair, $m_{t\bar{t}}$, (top) and for the total invariant mass of the process, $m_{Zt\bar{t}}$, (bottom). On the left (right) the pure signal contribution, S, to the $A \to HZ$ ($H \to AZ$) channel is shown, where H (A) decays to top quarks. The interference between the signal and box contributions is denoted by I.

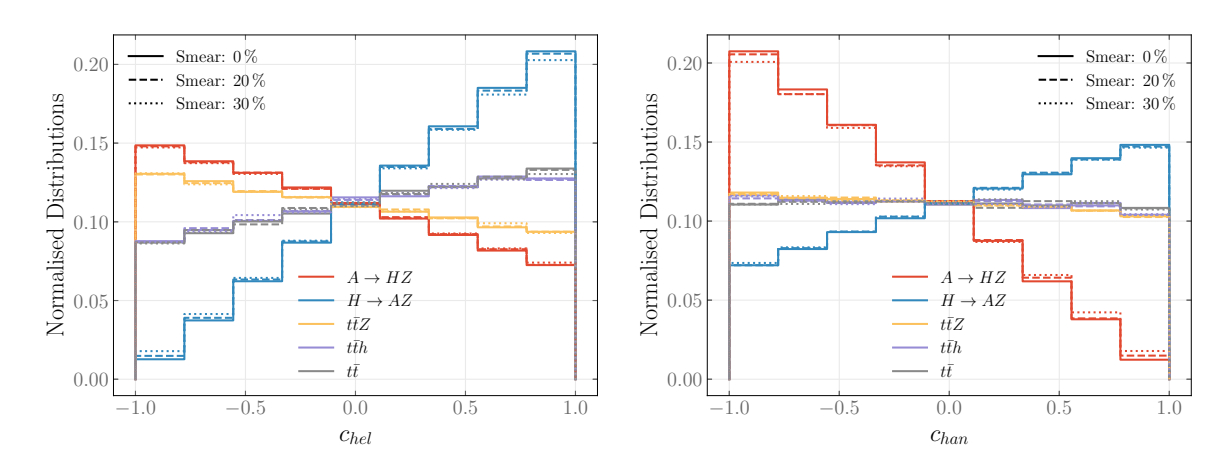


Figure 12. Distributions for c_{hel} and c_{han} with 0%, 20% and 30% smearing on the momenta of the MC-truth top and anti-top quarks. The $t\bar{t}Z$ background is shown, as well as the $A\to HZ$ and $H\to AZ$ channels with the lighter scalar decaying to $t\bar{t}$. For comparison, we also show distributions for $t\bar{t}$ and $t\bar{t}h$.

signal and background samples. We note that we do not smear the mass of the individual top quarks since it is usually kept fixed when experiments perform the algebraic reconstruction of the momenta [72]. The c_{hel} and c_{han} distributions for $A \to HZ \to t\bar{t}Z$, $H \to AZ \to t\bar{t}Z$ and $t\bar{t}Z$ are shown in figure 12 (we additionally show the distributions for $t\bar{t}$ and $t\bar{t}h$ for comparison). Overall, the impact from such shifts of the top-quark four-momenta is found to be small and we therefore do not include these effects in our analysis.

Data Availability Statement. This article has no associated data or the data will not be deposited.

Code Availability Statement. This article has no associated code or the code will not be deposited.

Open Access. This article is distributed under the terms of the Creative Commons Attribution License (CC-BY4.0), which permits any use, distribution and reproduction in any medium, provided the original author(s) and source are credited.

References

- [1] CMS collaboration, A portrait of the Higgs boson by the CMS experiment ten years after the discovery, Nature 607 (2022) 60 [arXiv:2207.00043] [INSPIRE].
- [2] ATLAS collaboration, A detailed map of Higgs boson interactions by the ATLAS experiment ten years after the discovery, Nature 607 (2022) 52 [Erratum ibid. 612 (2022) E24] [arXiv:2207.00092] [INSPIRE].
- [3] V.A. Kuzmin, V.A. Rubakov and M.E. Shaposhnikov, On the Anomalous Electroweak Baryon Number Nonconservation in the Early Universe, Phys. Lett. B 155 (1985) 36 [INSPIRE].
- [4] CMS collaboration, Searches for Higgs boson production through decays of heavy resonances, Phys. Rept. 1115 (2025) 368 [arXiv:2403.16926] [INSPIRE].
- [5] T. Biekötter et al., Fate of electroweak symmetry in the early Universe: Non-restoration and trapped vacua in the N2HDM, JCAP 06 (2021) 018 [arXiv:2103.12707] [INSPIRE].
- [6] D. Gonçalves, A. Kaladharan and Y. Wu, Resonant top pair searches at the LHC: A window to the electroweak phase transition, Phys. Rev. D 107 (2023) 075040 [arXiv:2206.08381] [INSPIRE].
- [7] T. Biekötter et al., The trap in the early Universe: impact on the interplay between gravitational waves and LHC physics in the 2HDM, JCAP 03 (2023) 031 [arXiv:2208.14466] [INSPIRE].
- [8] R. Mammen Abraham and D. Gonçalves, Boosting new physics searches in t̄Z and tZj production with angular moments, Eur. Phys. J. C 83 (2023) 965 [arXiv:2208.05986] [INSPIRE].
- [9] T. Biekötter et al., First shot of the smoking gun: probing the electroweak phase transition in the 2HDM with novel searches for $A \to ZH$ in $\ell^+\ell^-t\bar{t}$ and $\nu\nu b\bar{b}$ final states, JHEP **01** (2024) 107 [arXiv:2309.17431] [INSPIRE].
- [10] G.C. Dorsch, S.J. Huber, K. Mimasu and J.M. No, Echoes of the Electroweak Phase Transition: Discovering a second Higgs doublet through $A_0 \to ZH_0$, Phys. Rev. Lett. 113 (2014) 211802 [arXiv:1405.5537] [INSPIRE].

- [11] G.C. Dorsch, S.J. Huber, K. Mimasu and J.M. No, Hierarchical versus degenerate 2HDM: The LHC run 1 legacy at the onset of run 2, Phys. Rev. D 93 (2016) 115033 [arXiv:1601.04545] [INSPIRE].
- [12] J.M. Cline and P.-A. Lemieux, Electroweak phase transition in two Higgs doublet models, Phys. Rev. D 55 (1997) 3873 [hep-ph/9609240] [INSPIRE].
- [13] L. Fromme, S.J. Huber and M. Seniuch, Baryogenesis in the two-Higgs doublet model, JHEP 11 (2006) 038 [hep-ph/0605242] [INSPIRE].
- [14] P. Basler et al., Strong First Order Electroweak Phase Transition in the CP-Conserving 2HDM Revisited, JHEP 02 (2017) 121 [arXiv:1612.04086] [INSPIRE].
- [15] G.C. Dorsch, S.J. Huber, T. Konstandin and J.M. No, A Second Higgs Doublet in the Early Universe: Baryogenesis and Gravitational Waves, JCAP 05 (2017) 052 [arXiv:1611.05874] [INSPIRE].
- [16] D. Gonçalves, A. Kaladharan and Y. Wu, Electroweak phase transition in the 2HDM: Collider and gravitational wave complementarity, Phys. Rev. D 105 (2022) 095041 [arXiv:2108.05356] [INSPIRE].
- [17] L. Fromme and S.J. Huber, Top transport in electroweak baryogenesis, JHEP **03** (2007) 049 [hep-ph/0604159] [INSPIRE].
- [18] P. Basler, M. Mühlleitner and J. Wittbrodt, The CP-Violating 2HDM in Light of a Strong First Order Electroweak Phase Transition and Implications for Higgs Pair Production, JHEP 03 (2018) 061 [arXiv:1711.04097] [INSPIRE].
- [19] G.C. Dorsch, S.J. Huber, K. Mimasu and J.M. No, The Higgs Vacuum Uplifted: Revisiting the Electroweak Phase Transition with a Second Higgs Doublet, JHEP 12 (2017) 086 [arXiv:1705.09186] [INSPIRE].
- [20] W. Su, A.G. Williams and M. Zhang, Strong first order electroweak phase transition in 2HDM confronting future Z & Higgs factories, JHEP 04 (2021) 219 [arXiv:2011.04540] [INSPIRE].
- [21] ATLAS collaboration, Search for a CP-odd Higgs boson decaying into a heavy CP-even Higgs boson and a Z boson in the $\ell^+\ell^-t\bar{t}$ and $\nu\bar{\nu}b\bar{b}$ final states using 140 fb⁻¹ of data collected with the ATLAS detector, JHEP **02** (2024) 197 [arXiv:2311.04033] [INSPIRE].
- [22] CMS collaboration, Search for heavy neutral Higgs bosons A and H in the ttZ channel in proton-proton collisions at 13 TeV, Phys. Lett. B 866 (2025) 139568 [arXiv:2412.00570] [INSPIRE].
- [23] M. Bauer, M. Neubert and A. Thamm, Analyzing the CP Nature of a New Scalar Particle via S→Zh Decay, Phys. Rev. Lett. 117 (2016) 181801 [arXiv:1610.00009] [INSPIRE].
- [24] D0 collaboration, Evidence for spin correlation in tt production, Phys. Rev. Lett. 108 (2012) 032004 [arXiv:1110.4194] [INSPIRE].
- [25] CMS collaboration, Search for heavy Higgs bosons decaying to a top quark pair in proton-proton collisions at $\sqrt{s} = 13$ Tev, JHEP **04** (2020) 171 [Erratum ibid. **03** (2022) 187] [arXiv:1908.01115] [INSPIRE].
- [26] ATLAS collaboration, Search for heavy neutral Higgs bosons decaying into a top quark pair in $140 \, fb^{-1}$ of proton-proton collision data at $\sqrt{s} = 13 \, TeV$ with the ATLAS detector, JHEP 08 (2024) 013 [arXiv:2404.18986] [INSPIRE].
- [27] CMS collaboration, Search for heavy pseudoscalar and scalar bosons decaying to top quark pairs in proton-proton collisions at, CMS-PAS-HIG-22-013, CERN, Geneva (2024).

- [28] A. Anuar et al., ALP-ine quests at the LHC: hunting axion-like particles via peaks and dips in $t\bar{t}$ production, JHEP 12 (2024) 197 [arXiv:2404.19014] [INSPIRE].
- [29] B. Tweedie, Better Hadronic Top Quark Polarimetry, Phys. Rev. D 90 (2014) 094010 [arXiv:1401.3021] [INSPIRE].
- [30] Z. Dong, D. Gonçalves, K. Kong and A. Navarro, Entanglement and Bell inequalities with boosted tt, Phys. Rev. D 109 (2024) 115023 [arXiv:2305.07075] [INSPIRE].
- [31] T. Stelzer and S. Willenbrock, Spin correlation in top quark production at hadron colliders, Phys. Lett. B 374 (1996) 169 [hep-ph/9512292] [INSPIRE].
- [32] T.D. Lee, A Theory of Spontaneous T Violation, Phys. Rev. D 8 (1973) 1226 [INSPIRE].
- [33] J.-M. Gerard and M. Herquet, A twisted custodial symmetry in the two-Higgs-doublet model, Phys. Rev. Lett. 98 (2007) 251802 [hep-ph/0703051] [INSPIRE].
- [34] H. Bahl et al., HiggsTools: BSM scalar phenomenology with new versions of HiggsBounds and HiggsSignals, Comput. Phys. Commun. 291 (2023) 108803 [arXiv:2210.09332] [INSPIRE].
- [35] A. Djouadi, J. Kalinowski and M. Spira, HDECAY: A Program for Higgs boson decays in the standard model and its supersymmetric extension, Comput. Phys. Commun. 108 (1998) 56 [hep-ph/9704448] [INSPIRE].
- [36] HDECAY collaboration, HDECAY: Twenty₊₊ years after, Comput. Phys. Commun. **238** (2019) 214 [arXiv:1801.09506] [INSPIRE].
- [37] A. Barroso, P.M. Ferreira, I.P. Ivanov and R. Santos, Metastability bounds on the two Higgs doublet model, JHEP 06 (2013) 045 [arXiv:1303.5098] [INSPIRE].
- [38] W.G. Hollik, G. Weiglein and J. Wittbrodt, Impact of Vacuum Stability Constraints on the Phenomenology of Supersymmetric Models, JHEP 03 (2019) 109 [arXiv:1812.04644] [INSPIRE].
- [39] V. Cacchio, D. Chowdhury, O. Eberhardt and C.W. Murphy, Next-to-leading order unitarity fits in Two-Higgs-Doublet models with soft Z₂ breaking, JHEP 11 (2016) 026 [arXiv:1609.01290] [INSPIRE].
- [40] P. Bechtle et al., HiggsBounds: Confronting Arbitrary Higgs Sectors with Exclusion Bounds from LEP and the Tevatron, Comput. Phys. Commun. 181 (2010) 138 [arXiv:0811.4169] [INSPIRE].
- [41] P. Bechtle et al., HiggsBounds 2.0.0: Confronting Neutral and Charged Higgs Sector Predictions with Exclusion Bounds from LEP and the Tevatron, Comput. Phys. Commun. 182 (2011) 2605 [arXiv:1102.1898] [INSPIRE].
- [42] P. Bechtle et al., HiggsBounds 4: Improved Tests of Extended Higgs Sectors against Exclusion Bounds from LEP, the Tevatron and the LHC, Eur. Phys. J. C 74 (2014) 2693 [arXiv:1311.0055] [INSPIRE].
- [43] P. Bechtle et al., HiggsBounds-5: Testing Higgs Sectors in the LHC 13 TeV Era, Eur. Phys. J. C 80 (2020) 1211 [arXiv:2006.06007] [INSPIRE].
- [44] CMS collaboration, Search for charged Higgs bosons decaying into a top and a bottom quark in the all-jet final state of pp collisions at $\sqrt{s} = 13$ TeV, JHEP **07** (2020) 126 [arXiv:2001.07763] [INSPIRE].
- [45] ATLAS collaboration, Search for charged Higgs bosons decaying into a top quark and a bottom quark at $\sqrt{s} = 13$ TeV with the ATLAS detector, JHEP **06** (2021) 145 [arXiv:2102.10076] [INSPIRE].

- [46] CMS collaboration, Search for production of four top quarks in final states with same-sign or multiple leptons in proton-proton collisions at $\sqrt{s} = 13$ Tev, Eur. Phys. J. C 80 (2020) 75 [arXiv:1908.06463] [INSPIRE].
- [47] ATLAS collaboration, Search for $t\bar{t}H/A \to t\bar{t}t\bar{t}$ production in proton-proton collisions at $\sqrt{s} = 13$ TeV with the ATLAS detector, arXiv:2408.17164 [INSPIRE].
- [48] W. Bernreuther, D. Heisler and Z.-G. Si, A set of top quark spin correlation and polarization observables for the LHC: Standard Model predictions and new physics contributions, JHEP 12 (2015) 026 [arXiv:1508.05271] [INSPIRE].
- [49] A. Czarnecki, M. Jezabek and J.H. Kuhn, Lepton Spectra From Decays of Polarized Top Quarks, Nucl. Phys. B 351 (1991) 70 [INSPIRE].
- [50] A. Brandenburg, Z.G. Si and P. Uwer, QCD corrected spin analyzing power of jets in decays of polarized top quarks, Phys. Lett. B 539 (2002) 235 [hep-ph/0205023] [INSPIRE].
- [51] W. Bernreuther, A. Brandenburg, Z.G. Si and P. Uwer, Top quark pair production and decay at hadron colliders, Nucl. Phys. B 690 (2004) 81 [hep-ph/0403035] [INSPIRE].
- [52] J.A. Aguilar-Saavedra and J.A. Casas, Improved tests of entanglement and Bell inequalities with LHC tops, Eur. Phys. J. C 82 (2022) 666 [arXiv:2205.00542] [INSPIRE].
- [53] J. Rübenach, Search for heavy Higgs bosons in conjunction with neural-network-driven reconstruction and upgrade of the Fast Beam Condition Monitor at the CMS experiment, Ph.D. thesis, Universität Hamburg, 20146 Hamburg, Germany (2023) [INSPIRE].
- [54] B. Ravina, E. Simpson and J. Howarth, Observing t\(\bar{t}Z\) spin correlations at the LHC, Eur. Phys. J. C 81 (2021) 809 [arXiv:2106.09690] [INSPIRE].
- [55] J. Alwall et al., The automated computation of tree-level and next-to-leading order differential cross sections, and their matching to parton shower simulations, JHEP **07** (2014) 079 [arXiv:1405.0301] [INSPIRE].
- [56] R. Frederix et al., The automation of next-to-leading order electroweak calculations, JHEP 11 (2018) 085 [Erratum ibid. 11 (2021) 085] [arXiv:1804.10017] [INSPIRE].
- [57] N.D. Christensen and C. Duhr, FeynRules Feynman rules made easy, Comput. Phys. Commun. 180 (2009) 1614 [arXiv:0806.4194] [INSPIRE].
- [58] A. Alloul et al., FeynRules 2.0 A complete toolbox for tree-level phenomenology, Comput. Phys. Commun. 185 (2014) 2250 [arXiv:1310.1921] [INSPIRE].
- [59] C. Degrande et al., UFO The Universal FeynRules Output, Comput. Phys. Commun. 183 (2012) 1201 [arXiv:1108.2040] [INSPIRE].
- [60] L. Darmé et al., UFO 2.0: the 'Universal Feynman Output' format, Eur. Phys. J. C 83 (2023) 631 [arXiv:2304.09883] [INSPIRE].
- [61] M. Spira, A. Djouadi, D. Graudenz and P.M. Zerwas, Higgs boson production at the LHC, Nucl. Phys. B 453 (1995) 17 [hep-ph/9504378] [INSPIRE].
- [62] J. Kublbeck, M. Bohm and A. Denner, Feyn Arts: Computer Algebraic Generation of Feynman Graphs and Amplitudes, Comput. Phys. Commun. 60 (1990) 165 [INSPIRE].
- [63] T. Hahn, Generating Feynman diagrams and amplitudes with FeynArts 3, Comput. Phys. Commun. 140 (2001) 418 [hep-ph/0012260] [INSPIRE].
- [64] T. Hahn and C. Schappacher, The implementation of the minimal supersymmetric standard model in FeynArts and FormCalc, Comput. Phys. Commun. 143 (2002) 54 [hep-ph/0105349] [INSPIRE].

- [65] R.V. Harlander, S. Liebler and H. Mantler, SusHi: A program for the calculation of Higgs production in gluon fusion and bottom-quark annihilation in the Standard Model and the MSSM, Comput. Phys. Commun. 184 (2013) 1605 [arXiv:1212.3249] [INSPIRE].
- [66] R.V. Harlander, S. Liebler and H. Mantler, SusHi Bento: Beyond NNLO and the heavy-top limit, Comput. Phys. Commun. 212 (2017) 239 [arXiv:1605.03190] [INSPIRE].
- [67] C. Degrande, Automatic evaluation of UV and R2 terms for beyond the Standard Model Lagrangians: a proof-of-principle, Comput. Phys. Commun. 197 (2015) 239 [arXiv:1406.3030] [INSPIRE].
- [68] ATLAS collaboration, Inclusive and differential cross-section measurements of $t\bar{t}Z$ production in pp collisions at $\sqrt{s} = 13$ TeV with the ATLAS detector, including EFT and spin-correlation interpretations, JHEP 07 (2024) 163 [arXiv:2312.04450] [INSPIRE].
- [69] J. Alwall et al., A standard format for Les Houches event files, Comput. Phys. Commun. 176 (2007) 300 [hep-ph/0609017] [INSPIRE].
- [70] D0 collaboration, Measurement of the top quark mass using dilepton events, Phys. Rev. Lett. 80 (1998) 2063 [hep-ex/9706014] [INSPIRE].
- [71] CMS collaboration, Measurement of Differential Top-Quark Pair Production Cross Sections in pp collisions at $\sqrt{s} = 7$ TeV, Eur. Phys. J. C 73 (2013) 2339 [arXiv:1211.2220] [INSPIRE].
- [72] CMS collaboration, Measurement of the differential cross section for top quark pair production in pp collisions at $\sqrt{s} = 8$ TeV, Eur. Phys. J. C 75 (2015) 542 [arXiv:1505.04480] [INSPIRE].
- [73] G. Cowan, K. Cranmer, E. Gross and O. Vitells, Asymptotic formulae for likelihood-based tests of new physics, Eur. Phys. J. C 71 (2011) 1554 [Erratum ibid. 73 (2013) 2501] [arXiv:1007.1727] [INSPIRE].